J3.4A HIGH-RESOLUTION SIMULATIONS OF THE URBAN ATMOSPHERE IN SEA-BREEZE CONDITIONS

Isabelle Calmet *, Sylvie Leroyer and Patrice G. Mestayer
Laboratoire de Mécanique des Fluides, UMR 6598 CNRS-Ecole Centrale de Nantes, France

1. INTRODUCTION

Large-eddy simulations of the dynamics and the thermodynamics of the boundary layer over Marseille (France) during the Intensive Observation Period (IOP) 2b of the UBL-Escompte experiment (Mestayer et al., 2005) have been performed with the SUBMESO atmospheric model derived from ARPS (Xue et al, 2000). The IOP 2b (from June 24 to June 26, 2001) is characterized by sunny weather with light winds which facilitate the sea-breeze development and its penetration inland. The south-westerly sea-breeze on June 24 is replaced at night by the north-westerly regime, a remnant of the previous days but with a smaller intensity. On June 25 and 26 a southerly regime extends over the whole region.

A large amount of data has been collected during UBL-Escompte. Five sites were equipped with meteorological masts to measure the radiative and turbulent fluxes (red symbols on Fig. 1) while an array of twenty temperature-humidity sensors was deployed, at 6 m above ground level (agl) (blue symbols on Fig. 1). Numerous works have been devoted to the numerical simulation of this campaign allowing to study the pollutant dispersion or the urban heat island of this coastal city (e.g., Lemonsu et al., 2005). Flux measurements at the city centre have been used to validate separately the energy budget models (LUMPS, TEB or SM2U). The SM2U soil model (Dupont & Mestayer, 2006) is used here in coupling with the atmospheric model to account for specific urban processes.

The present work focuses on June 24. The first aim is to assess the accuracy of the simulation results and our choices of large-scale forcing and of surface/canopy description. The second objective is to investigate the competing influences of the sea-breeze and of the urban physical processes.

2. MODEL SET UP AND EVALUATION

Simulations are performed on two nested domains (Fig.1). The first one (G1) has a 990 m horizontal resolution and covers a large region half of which is Mediterranean Sea. The second one (G2) covers the whole town of Marseille with a 330 m resolution. The sea surface temperature (SST) is derived from the satellite data (Mc Clain et al.,1985) available at midnight on June 23 and at noon on June 25 (Dousset & Kermadi, 2003). The SST is computed at each time step as a function of the solar radiation and of the diurnal amplitude. The land use and the aerodynamic and morphological parameters of the city are determined from the French urban database BDTopo provided by IGN. Figure 2 presents the urban fabric classification in typical districts (Long & Kergomard 2005). The most urbanized districts are located near the coast and the city extends inland on hill slopes and along two valleys. The simulation begins at 00:00 UTC on June 24 and results are shown from 04:00 UTC since the first hours data are dependent on initial conditions. The hourly outputs of the mesoscale model RAMS (Taghavi et al., 2004) are used as inflow conditions on the G1 boundaries.

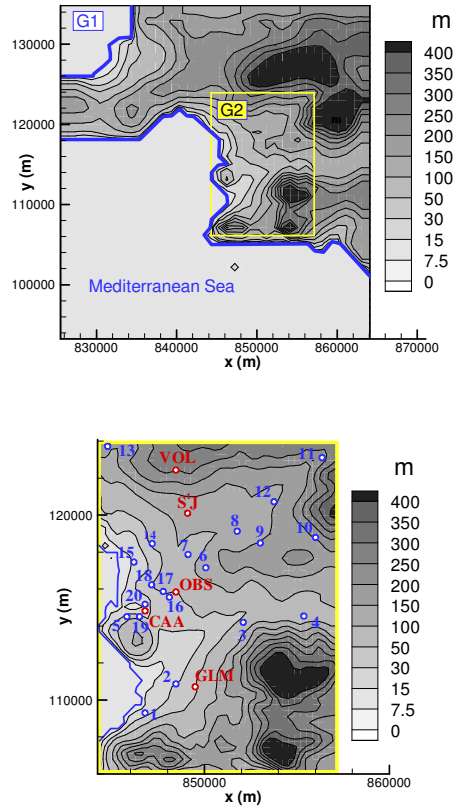

Figure 1: Top: Topography and simulation domains. Bottom: Measurement points and topography at 330 m resolution on G2 domain.

* *Corresponding author address*: Isabelle Calmet, Laboratoire de Mécanique des Fluides, UMR 6598 CNRS-Ecole Centrale de Nantes, B.P. 92101, 44321 Nantes Cedex 3, France.
E-mail : isabelle.calmet@ec-nantes.fr

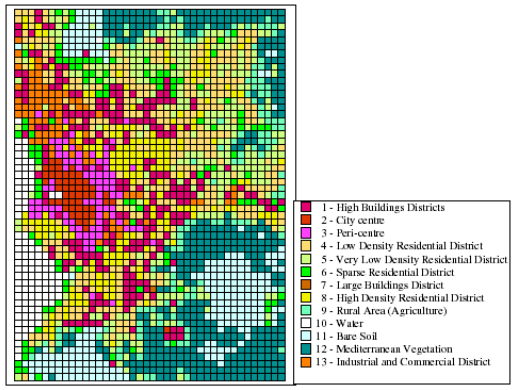

Figure 2: Urban fabric classification at 330 m resolution (G2 grid)

Figures 3 and 4 compare the measured and simulated (first grid mesh above the ground) wind velocity and direction at the city centre and in a residential district inland (CAA and STJ sites, respectively). The north-east wind blowing at night is replaced by a westerly wind after 06:30 UTC. The transition to the sea-breeze regime is also identified by a wind velocity drop. On both sites, the maximum velocity is reached around 13:00 UTC. At CAA the wind is lower than at STJ, leading to a high variability in the wind direction measurement. The model being unable to produce these fluctuations, the simulation results are better (both for velocity and direction) at STJ than at CAA. Indeed, a constant western direction is simulated during the daytime instead of the north-west direction expected when the measured wind is not negligible. At CAA wind velocity differences appear on both G1 and G2 simulations. This is probably due to the low resolution on G1 where the mesh including the CAA is close to - and over-influenced by - the sea.

Figure 5 represents the measured air temperature at 6 m agl and the simulated temperature at 7.5 m agl at the points 4, 14, 7, 8 and 12 of Fig.1. The point 14 is in a densely urbanized district very close to the coast. Points 7, 8 and 12 are located in the plain that extends from the city centre to the north-east part of the G2 domain. The point 4 is in a suburban district far inland and not directly submitted to sea breeze influence. In the middle of the day, both measurement and simulation show a temperature raise from the coast to the land. A one-hour phase lag is observed in the temperature raise in the morning and drop in the late afternoon for stations the less influenced by the breeze. This can be explained by a possible underestimation of the surface humidity (not measured), inducing a too fast model reaction to solar radiation for the natural soils and then to fast variations of air temperature at sunrise and sunset. This default may also be responsible for the very low temperatures at night in the simulations.

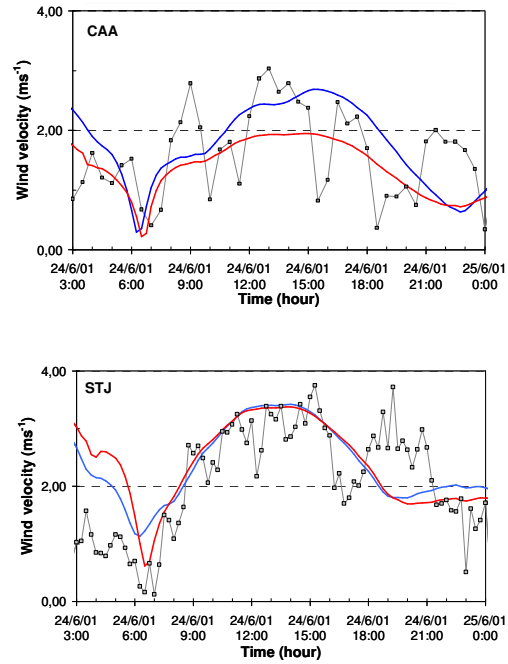

Figure 3: Wind velocity (measurements in black, simulations on G1 in blue and on G2 in red) at CAA (top) and STJ (bottom).

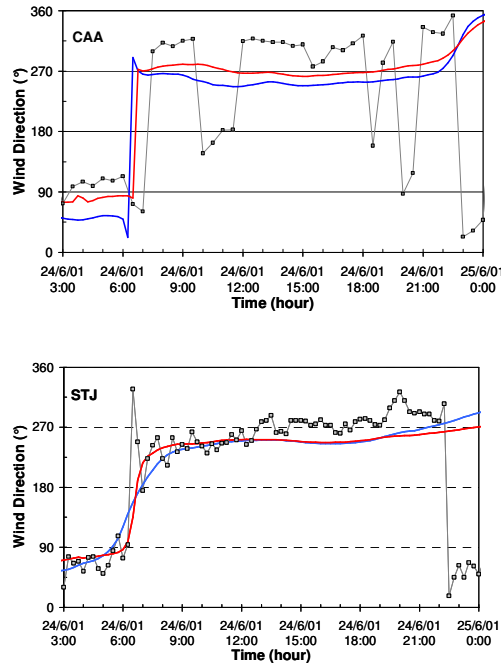

Figure 4: Wind direction (measurements in black, simulations on G1 in blue and on G2 in red) at CAA (top) and STJ (bottom).

The observation of the energy budget at OBS (not shown) confirms this hypothesis. While the latent heat flux is expected to be very low at the CAA (Fig.6), it is 100 Wm^{-2} at the warmest hours of the day at OBS due to the neighboring of a vegetated park that may have been watered. The other terms of the simulated energy budget are in quite good agreement with the observations.

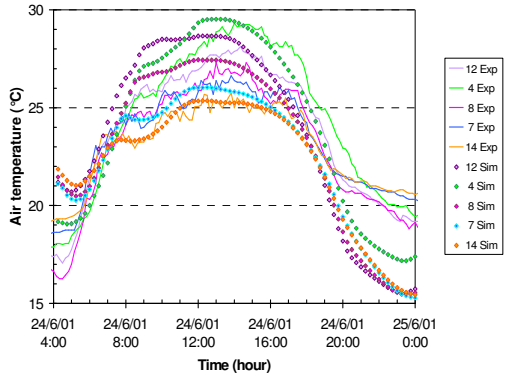

Figure 5: Air temperature at the Points 4, 7, 8, 12 and 14 of Figure 1. (measurements, lines ; simulation on G2, symbols).

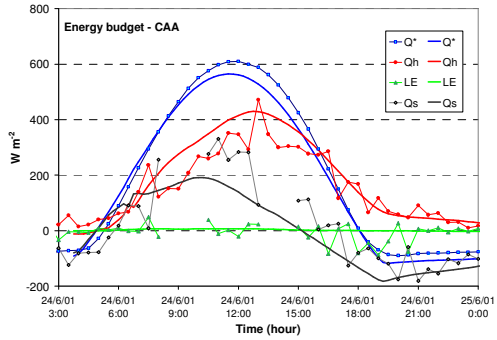

Figure 6: Energy budget at CAA (measurements, symbols; simulation on G2, lines).

3. BREEZE ANALYSIS

The simulation results are presented at 13:00 UTC for both grids on Fig. 7 at 7.5 m agl. The temperature gradient from the coast to the land is observed as previously stated. The main sea-breeze penetrates through the west coast leading to temperature iso-values nearly parallel to the coastline on the first two kilometers. The wind vertical profiles at different locations along the streamline (drawn in blue on Fig.7) are shown on Fig. 8 (left). Along this streamline, we can observe that the wind first decelerates over the land due to sea-city transition. As the most urbanized (and most rough) districts are located near the coast, the wind tends to accelerate again as the distance from the coast increases. Further inland the wind velocity becomes again comparable to the wind velocity over the sea. Fig. 8 (right) shows the potential temperature evolution with the distance from the coast. A thermal internal boundary layer develops due to both the warming of the surfaces and the penetration of the breeze inland. This leads to a strongly convective layer near the surface, capped by the stratified layer already observed upstream. The convective layer growth is only 50 m high between points 18 and 10. The temperature profiles collapse above 350 m while the wind field is still disturbed at this altitude, due to topography influence.

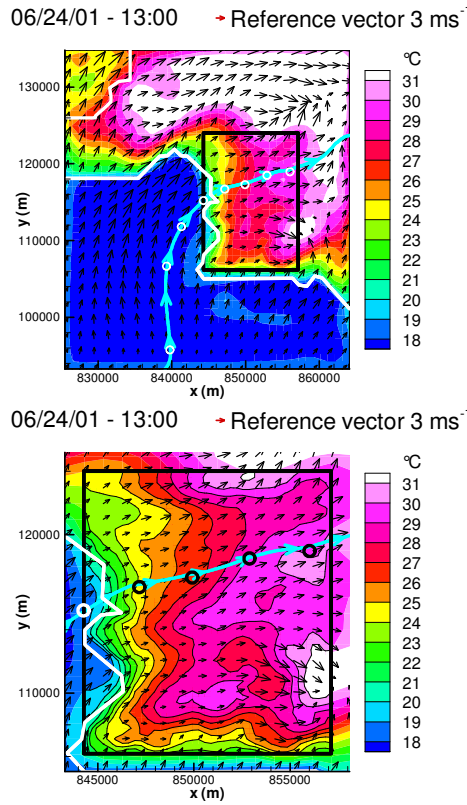

Figure 7: Temperature and wind field at 13:00 UTC at 7.5 m agl on G1 (top) and G2 (bottom). The blue line represents a streamline. The circles on the bottom frame show the locations of Figs. 8-9 profiles; they correspond to points 18, 6, 9 and 10 of Fig. 1.

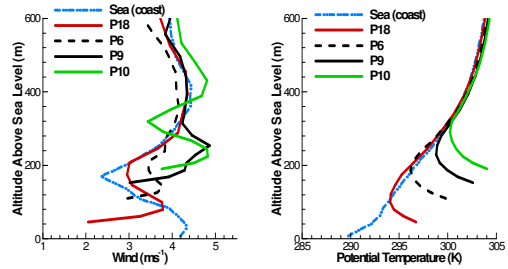

Figure 8: Vertical profiles of mean wind (left) and potential temperature (right) along Fig. 7 streamline (bottom). The profiles are averaged over 30 minutes from 12:45 – 13:15.

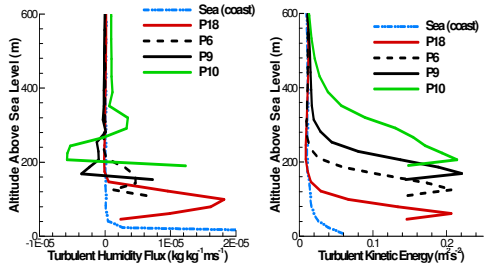

Figure 9: Vertical profiles of turbulent humidity flux (left) and turbulent kinetic energy (right) along the streamline of Fig. 7 (bottom). The profiles are averaged over 30 minutes from 12:45 – 13:15.

The profiles of turbulent humidity flux and turbulent kinetic energy (TKE) are shown on Fig. 9. All the TKE profiles over land present the same maximum value at the altitude corresponding to one third of the convective layer depth. At higher altitudes agl, the TKE raises all the more as the distance from the coast increases. As it could be expected, the penetration of humid air, brought by the sea-breeze, influences the humidity turbulent flux near the coast above the convective layer.

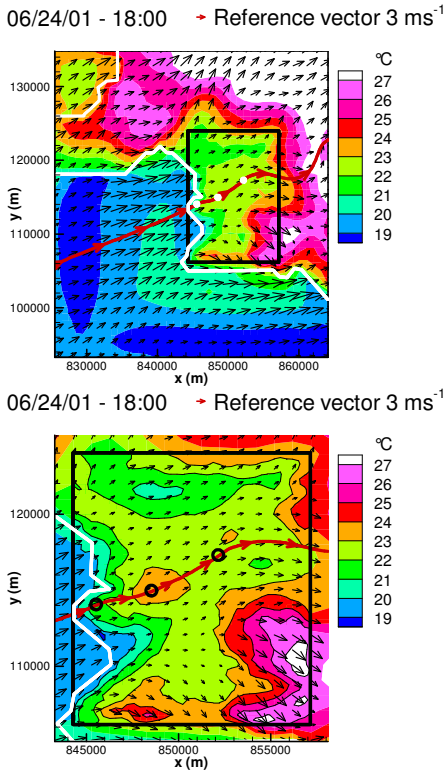

Figure 10: Temperature and wind fields at 18:00 UTC at 7.5 m agl on G1 (top) and G2 (bottom). The red line represents a streamline. The circles on the bottom frame show the locations of Figs. 11-12 profiles.

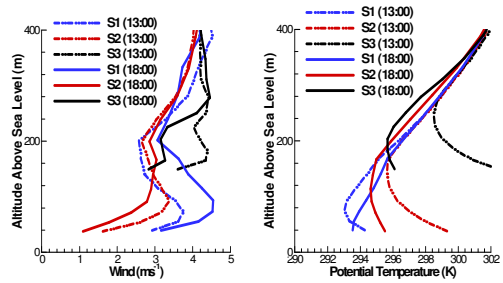

Figure 11: Vertical profiles of mean wind (left) and mean potential temperature (right) along the streamline of Fig. 10 (bottom). The profiles are averaged over 30 minutes around the indicated times.

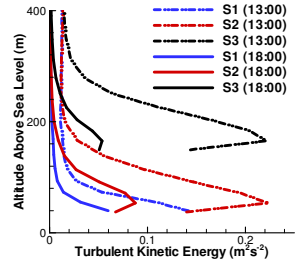

Figure 12: Vertical profiles of turbulent kinetic energy along the streamline of Fig. 10 (bottom). The profiles are averaged over 30 minutes around the indicated times.

Figure 10 shows the simulation results at 18:00 UTC for both grids at 7.5 m agl. The evolution of the vertical profiles, both in time and along a streamline (Fig. 10), is shown on Figs. 11-12 for the wind, the potential temperature and the TKE. Due to surface cooling, at 18:00 the air temperature is more homogeneously distributed than at 13:00. At the same time, the wind velocity drops over land as well as the TKE. The thermal footprint of the densely urbanized coastal zones is apparent in the G2 results (Fig. 10, bottom). This is correlated with the lower layers stratification with is stable at the coast but slightly convective over the city (Fig. 11, right). Note that the TKE maximum value is higher over the city centre than over residential districts.

4. CONCLUSION

The studied region is particularly complex due to both high topographical variations very close to the sea and coastal urbanization. Numerical simulation is especially useful here to understand the interactive dynamical and thermal processes. The objective of this study was a first analysis of the competing influences of the sea-breeze and of the urban boundary layer. The availability of experimental data at different locations on the site allows to validate or to criticize the simulation results. At the city scale, the regional forcing is obviously very important since it generates the large-scale situation influencing the breeze development. Here, the uncertainty on inflow conditions has to be accounted for, particularly over the sea where no measurements are available. It is also the case for the SST that has been crudely estimated while it is of great importance in the breeze process. Another crucial parameter is the

surface (and soil) humidity, when the main diurnal forcing comes from the warming and cooling of the surfaces. Other simulations will be performed in order to test the sensitivity to a heterogeneous repartition of the humidity, considering that some natural surfaces of urbanized districts are artificially watered.

5. ACKNOWLEDGEMENTS

This study was partly supported by CNRS/INSU grant PATOM 2005 51/0576 and Ministry of Environment PRIMEQUAL2-PREDIT grant R2. The computer resources were provided by the Centre Informatique National de l'Enseignement Supérieur (CINES).

6. REFERENCES

Dousset B and S. Kermadi, 2003: Satellites Observation over the Marseille-Berre area during the UBL/CLU-ESCOMPTE experiment, Proc. 5th Int. Conf. Urban Climate, 1-5 Sept. 2003, Lodz, Poland, 323-326

Dupont, S. and Mestayer, P. G., 2006: Parameterization of the Urban Energy Budget with the submesoscale soil model, *J. Appl. Meteor. Climatol.,* **45**, 1744-1765

Lemonsu A., Pigeon G., Masson V. and Moppert C., 2006: Sea town interactions over Marseille: 3D urban boundary layer and thermodynamic fields near the surface, *Theor. Appl. Climatol.* **84**, 171–178

Long, N. & C. Kergomard, 2005: Classification morphologique du tissus urbain pour des applications climatologiques; Cas de Marseille, *Revue Internationale de Géomatique*, **15**, 487-512

McClain, E. P., Pichel, W.G. and Walton, C. C., 1985: Comparative Performance of AVHRR-Based Multichannel Sea Surface Temperatures', *J. Geophys. Res*., **90**, 11587-11601

Mestayer, P. G., P. Durand and co-authors, 2005: The Urban Boundary Layer Field Experiment over Marseille. UBL/CLU-ESCOMPTE: Experimental Set-up and First Results, *Boundary-Layer Meteor*. **114**, 315-365.

Taghavi, M., S. Cautenet, G. Forest, 2004: Simulation of ozone production in a complex circulation region using nested grids, *Atmosph. Chem. and Phys.* **4**, 825-838.

Xue, M., Droegemeier, K. K., and Wong, V., 2000: The Advanced Regional Prediction System (ARPS) – multi-scale nonhydrostatic atmospheric simulation and prediction model. Part I: Model dynamics and verification, *Meteor. and Atmos. Phys.* **75**, 161-193.